DOI: https://doi.org/10.2138/am-2020-7393

Revision 1

Donwilhelmsite, [$CaAl_4Si_2O_{11}$], a new lunar high-pressure Ca-Al-silicate with relevance for subducted terrestrial sediments

Jörg Fritz[1,2], Ansgar Greshake[3], Mariana Klementova[4], Richard Wirth[5], Lukas Palatinus[4], Reidar G. Trønnes[6], Vera Assis Fernandes[3,7], Ute Böttger[8], and Ludovic Ferrière[9]

[1]Zentrum für Rieskrater und Impaktforschung, Nördlingen, Vordere Gerbergasse 3
86720 Nördlingen, Germany

[2]Saalbau Weltraum Projekt, Liebigstraße 6, D-64646 Heppenheim, Germany

[3]Museum für Naturkunde Berlin, Invalidenstraße 43, D-10115 Berlin, Germany

[4]Institute of Physics of the Czech Academy of Science, v.v.i., Na Slovance 2, 182 21 Prague, Czech Republic

[5]Helmholtz-Zentrum Potsdam - Deutsches GeoForschungsZentrum, Sektion 3.5 Grenzflächen-Geochemie, Telegrafenberg, D-14473 Potsdam, Germany

[6]Natural History Museum and Centre for Earth Evolution and Dynamics (CEED), University of Oslo, N-0315 Oslo, Norway

[7]Department of Earth and Environmental Sciences, University of Manchester, Williamson Building, Oxford Road, M13 9PL Manchester, United Kingdom

[8]Institut für Optische Sensorsysteme, Deutsches Zentrum für Luft und Raumfahrt Berlin, Rutherfordstraße 2, D-12489 Berlin, Germany

[9]Natural History Museum, Burgring 7, A-1010 Vienna, Austria

E-mail of corresponding author: joerg.fritz@kino-heppenheim.de

ABSTRACT

We report on the occurrence of a new high-pressure Ca-Al-silicate in localized shock melt pockets found in the feldspatic lunar meteorite Oued Awlitis 001 and discuss the implications of our discovery. The new mineral crystallized as tiny, micrometer sized, acicular grains in rock-melt pockets of roughly anorthitic bulk composition. Transmission electron microscopy based 3 dimension electron diffraction (3D ED) revealed that the $CaAl_4Si_2O_{11}$ crystals are identical to the calcium aluminum silicate, CAS, phase first reported from static pressure experiments. The new mineral has a hexagonal structure, with a space group *of* $P6_3/mmc$ and lattice parameters of a = 5.42(1) Å; c = 12.70(3) Å; V = 323(4) Å^3; Z = 2. This is the first time 3D ED was applied to structure determination of an extraterrestrial mineral. The International Mineralogical Association has approved this naturally formed CAS phase as the new mineral "donwilhelmsite" [$CaAl_4Si_2O_{11}$], honoring the lunar US geologist Don E. Wilhelms. On the Moon, donwilhelmsite can form from the primordial feldspathic crust during impact cratering events. In the feldspatic lunar meteorite Oued Awlitis 001 needles of donwilhelmsite crystallized in ~200 µm in size shock melt pockets of anorthositic-like chemical composition. These melt pockets quenched within milliseconds during declining shock pressures. Shock melt pockets in meteorites serve as natural crucibles mimicking the conditions expected in the Earth' mantle. Donwilhelmsite forms in the Earths' mantle during deep recycling of aluminous crustal materials, where it is a key host for Al and Ca of subducted sediments in most of the transition zone and in the uppermost lower mantle (460-700 km). Donwilhelmsite bridges the mineralogical gap between kyanite and the Ca-component of clinopyroxene at low pressures and the Al-rich Ca-ferrite phase and Ca-perovskite at high-pressures. In ascending buoyant mantle plumes, at about 460 km depth, donwilhelmsite is expected to break down into minerals such as garnet, kyanite, and clinopyroxene. This may trigger minor partial melting releasing a range of incompatible minor and trace elements contributing to the enriched mantle (EM1 and EM2) components associated with subducted sedimentary lithologies.

Keywords: High-pressure phase, new mineral, donwilhelmsite, Oued Awlitis 001 lunar meteorite, shock metamorphism, subduction, mantle mineral, enriched mantle component

INTRODUCTION

The Earth's continental crust and the lunar highlands (i.e., consisting of material derived from many superposed impact ejecta from all crustal levels and covering the lunar surface) are dominantly felsic in composition, including as major elements, O, Si, Al, Ca, Na, and K. Minerals controlling the distribution of these elements are important agents for the origin and fate of planetary crusts. Remnants of a primordial crust are preserved on the Moon, showing the intense mechanical and thermal metamorphism and melting, caused by impacts during the Heavy Bombardment Eon (Wilhelms 1987; Fernandes et al. 2013). Nonetheless, these remnants document initial planetary differentiation processes. Fifty years ago, the Apollo 11 mission collected 21.6 kg of lunar rocks and soils, including anorthosites composed of >90 vol% plagioclase (Wilhelms 1987, 1993). Lunar anorthosites contain exceptionally high proportions of the Ca-rich anorthite endmember of the albite – anorthite ($Na[AlSi_3O_8]$ – $Ca[Al_2Si_2O_8]$) plagioclase solid solution, with 96-98 mol% anorthite. From these samples, it was concluded that the impact gardened bright lunar highlands derived from a primordial (>4.3 Ga old) anorthositic crust, several tens of kilometers thick (50 ± 15 km, e.g., Wieczorek et al. 2006) that crystallized and floated on a dense lunar magma ocean, several hundred kilometers deep (Wood et al. 1970; Smith et al. 1970).

Preservation of a highly fragmented and displaced primary crust (>4.4 Ga), as well as primary mantle heterogeneities resulting from the crystallization of the, likely heterogeneous, lunar magma ocean, is in stark contrast to the geologically active Earth. Earth's oldest preserved oceanic and continental crusts are about 0.2 and 4.0 Gy old, respectively, with the latter being found in very limited areas on Earth. During plate tectonic processes, crustal materials rich in volatiles and other elements incompatible in mantle minerals are reintroduced into the depleted mantle by subduction. The sinking oceanic plates carry continental-derived sediments into the deep mantle (Irifune et al. 1994; Plank and Langmuir 1998), and the enriched mantle component EM2 (enriched mantle 2; with high $^{87}Sr/^{86}Sr$ and intermediate $^{206}Pb/^{204}Pb$) is ascribed to the direct terrigenous component with a composition similar to the upper continental crust (White 2015). In contrast, the origin of the enriched mantle component EM1 (enriched mantle 1; with intermediate $^{87}Sr/^{86}Sr$ and low $^{206}Pb/^{204}Pb$) is more elusive but often attributed to pelagic sediments (Garapić et al. 2015). Especially Archean-aged sediments are good candidates for the enriched components in the mantle source of South Pacific Ocean islands like Pitcairn (Delavault et al. 2016). About 75% of the subducted sediment flux is estimated to be direct terrigenous material of average upper crust composition (Plank and Langmuir 1998). Such lithologies can be recycled into the lower mantle and retained there for up to 2-3 Gy, before being sampled by recent plumes and ongoing ocean island volcanism. Deep recycling of continentally derived sediments below 200-300 km depth is facilitated by stepwise densification at 6.5 GPa (~200 km depth), when orthoclase breaks down, and at 9 GPa (~300 km depth), when hollandite and stishovite form, to densities exceeding that of ambient peridotite at the 280-700 km depth range (Irifune et al. 1994). At deeper levels, the sediment and peridotite densities may remain nearly identical to depths beyond 1200 km and ~40 GPa (Poli and Schmidt 2002). The densification of terrigenous and pelagic sedimentary lithologies in the mantle transition zone is aided by the occurrence of 7-10 % of a Ca-Al-silicate (CAS) phase with composition $CaAl_4Si_2O_{11}$ at the 460-700 km depth range (Irifune et al. 1994).

Natural examples of those minerals composing Earths' deep mantle are rarely accessible. Many minerals stable at deep mantle pressure and temperature conditions decompose into other mineral assemblages stable at lower pressures due to the specific pressure-temperature-time (P-T-t) path during ascent. Notable exceptions include high-pressure phases such as ringwoodite (high-pressure polymorph of olivine), ferropericlase, and Mg-wüstite found as inclusions in diamonds (e.g., Pearson et al. 2014). The diamond host serves as a pressure vault providing an environment that allows deep mantle high-pressure mineral inclusions to cool to temperatures low enough to inhibit a back reaction into low-pressure mineral assemblages. Localized zones of shock melt in moderately to strongly shocked meteorites present another natural environment in which a hot and compressed melt is quenched at typical deep mantle pressures to temperatures low enough to inhibit a back reaction into low-pressure mineral assemblages during pressure release (Chen et al. 1996; Fritz et al. 2017). A great diversity of natural examples of high-pressure minerals, analogous to those occurring in the Earths' mantle, were first found in local shock melt zones (such as melt veins and melt pockets) of different types of meteorites, including chondrites and achondrites of basaltic and dunitic compositions (e.g., Tomioka and Miyahara 2017). Compared to mafic and ultramafic meteorites, reports of shock melt zones in felsic meteorites are very limited. Although CAS-like phases of various compositions close to the $CaAl_4Si_2O_{11}$-$NaAl_3Si_3O_{11}$ have been found in shocked basaltic meteorites from Mars (i.e., in shergottites, Beck et al. 2004; El Goresy et al. 2013), the CAS phase has neither been characterized in felsic meteorites, nor been officially named. Here we report on the discovery and detailed characterization of the natural high-pressure and high-temperature transformation of anorthite in shock melt zones within the feldspathic lunar meteorite Oued Awlitis 001.

MATERIAL AND METHODS

Oued Awlitis 001 meteorite

The main fragment of the lunar meteorite Oued Awlitis 001, originally 382 g, was found on January 15, 2014, in the Western Sahara (25.954°N, 12.493°W). It is largely covered with a green to brownish fusion crust showing features of orientation. Another fragment, 50.5 g, fitting the larger one, was found a few weeks later. About 60% of the recovered meteorite is covered with a crackled fusion crust and shows a rollover lip on one side. Oued Awlitis 001 is classified as an anorthositic lunar impact melt rock, composed of large anorthite clasts set in a poikilitic matrix of plagioclase, olivine, and pyroxene (Ferrière et al. 2017; Ruzicka et al. 2017; Wittmann et al. 2019). The poikilitic matrix indicates a slow cooling history, possibly in a ~100 meter thick impact melt sheet (Wittmann et al. 2019). Later impact event(s) emplaced the rock closer to the lunar surface, and about 0.3 Ma ago it was impact accelerated beyond lunar escape velocity and delivered to Earth (see Ferrière et al. 2017; Wittmann et al. 2019). The sections investigated in this study were prepared from the 50.5 g fragment of this meteorite from the Natural History Museum Vienna (NHMV, Austria) collection (specimen NHMV-N9830).

Optical microscopy

A thin section of Oued Awlitis 001 (NHMV-O105), prepared from the pristine part of the meteorite (i.e., excluding the fusion crust) was studied in transmitted light at the NHMV. A polished thick section mounted in epoxy (NHMV-O104) was studied by optical microscopy in reflected light aided by the use of immersion oil at the Museum für Naturkunde, Berlin, Germany. Such an approach is ideal to recognize potential high-pressure phases within local shock melt zones inside meteorites, as minerals and glass display intense brightness contrast in reflected light. This thick section was then studied using a binocular microscope, to acquire depth information of the transparent minerals and their outer surface, visible through the transparent epoxy mount.

Micro-Raman spectroscopy

Subsequently, micro-Raman spectroscopic analyses were conducted on the uncoated thick section and prior to any disturbances caused by electron beam irradiation during electron microscopic investigations. Raman spectra were collected with the WITec Alpha 300 Raman confocal microscope at the Deutsches Zentrum für Luft und Raumfahrt (DLR), Berlin, Germany, using a Nd:YAG laser with an excitation wavelength of 532 nm, a 100x magnification objective (NA 0.8), and a power of 3 to 7 mW on the sample.

Electron microscopy

Backscattered electron (BSE) microscopic images were obtained on the polished and carbon coated thick section at the Museum für Naturkunde Berlin (MfN), Germany, using a JEOL JXA 8500F Field Emission Microprobe. For X-ray elemental maps, the microprobe was operated with 15 kV accelerating voltage, a 15 nA beam current, an about 10 nm beam size, and a dwell times of 100 ms. Quantitative chemical analyses of the shock melt pocket were obtained with the same instrument using a 10–15 kV accelerating voltage, a 15 nA beam current, and a defocused 10 µm diameter beam. Suitable glass and mineral standards certified by the Smithsonian Museum were used as reference samples for electron microprobe analysis (Jarosewich et al. 1980).

Focused Ion Beam (FIB)

FIB foils 20 x 10 x 0.15 µm in size were cut out of the thick section at the Deutsches GeoForschungsZentrum, Sektion 3.5 Grenzflächen-Geochemie Helmholtz-Zentrum (GFZ) Potsdam, Germany, using a FEI TEM 200 FIB system.

Transmission electron microscopy (TEM)

Initial TEM characterization was performed using a FEI Tecnai™ G2 F20 X-Twin operated at 200 kV with a field emission gun electron source at GFZ Potsdam. The microscope is equipped with an EDAX ultra-thin window EDX system, a Fishione high-angle annular dark-field (HAADF) detector, and a post-column Gatan imaging filter (GIF Tridiem).

Additional TEM characterization, including chemical analyses and crystal structure determination, was performed at the Institute of Physics of the Czech Academy of Science (IPCAS), Prague, Czech Republic. The reported chemical analyses were obtained using an FEI Tecnai™ G2 F20 X-Twin attached with an EDAX energy dispersive spectrometer (EDS) operated at 200 kV. The chemical analyses were obtained with a defocused beam with the size of about 300 nm in diameter in TEM mode to avoid the loss of volatile elements such as sodium. Standardless quantification using FEI TIA software version 4.2 was used for the analysis. The empirical formula was calculated on the basis of 7 cations.

The crystal structure of donwilhelmsite was determined by 3D electron diffraction (3D ED; Gemmi et al. 2019 and references therein) performed on a Philips CM 120 (LaB_6, 120kV), equipped with a NanoMEGAS precession unit DigiStar and an Olympus SIS CCD camera Veleta (2048 x 2048 px), in Prague. The diffraction data were collected by means of precession electron diffraction (Mugnaioli et al. 2009). The target crystal was sequentially tilted by 1 deg. step from -50 to +50 deg., and at every tilt step a precession diffraction pattern in micro-diffraction mode was acquired using a precession angle of 1 deg. Data processing was carried out using the PETS software (Palatinus et al. 2019). Structure solution and refinement were performed using the computing system Jana2006 (Petříček et al. 2014). The structure was solved by the charge flipping algorithm using the program Superflip (Palatinus and Chapuis 2007), and refined using a dynamical approach (Palatinus et al. 2015a, 2015b).

RESULTS

The feldspathic lunar meteorite Oued Awlitis 001 (Fig. 1) is an impact melt rock predominantly composed of up to about 5 mm-sized Ca-rich plagioclase clasts set into a crystallized melt groundmass composed of <100 µm sized olivine and pyroxene grains poikilitically enclosing equally sized anorthite grains. All silicates display strong compositional zoning. Minor phases present include FeNi metal, troilite, ilmenite, Ti-rich spinel, apatite, zircon, baddeleyite, and silica. For the detailed petrology and mineral chemistry of the meteorite the reader is referred to Ferrière et al. (2017) and Wittmann et al. (2019).

Oued Awlitis 001 is moderately shocked. The observed shock metamorphic effects developed during a later impact event which affected the already fully crystalline impact melt rock. Plagioclase is mostly crystalline, showing undulatory extinction, reduced birefringence, and well-developed planar deformation features (PDF). In a few places, the plagioclase is transformed into diaplectic glass, so-called maskelynite.

Locally, the meteorite contains thin shock melt veins ranging from 50 to 150 µm in thickness, as well as shock melt pockets with diameter typically of about 200 µm (Fig. 2a). Optical inspection with a binocular microscope showed that the melt veins are three dimensional melt sheets with irregular surfaces extending deep into the meteorite sample. The melt veins are recrystallized to extremely fine-grained mineral assemblages. In contrast, the melt pockets appear isolated and contain bundles (acicular texture) of up to 20 µm long and less than 1 µm wide needles that crystallized from the melt (Fig. 2b). Electron microprobe investigation revealed that the shock melt pockets are roughly anorthitic in bulk composition (Table 1). In high-contrast BSE images (Fig. 2a-b), the acicular crystals appear slightly brighter than the matrix and are surrounded by a comparatively darker halo when compared to the adjacent anorthite shock melt. Elemental maps show that the needle shaped crystals are enriched in Al and slightly depleted in Ca compared to the glass in the shock melt pocket (Fig. 3). The needles do not incorporate Fe and Mg (the Mg map is not shown). The compositional differences between glass and crystals are such that these phases can be easily overlooked in low-contrast BSE surveys. The localized zones of shock melt and the potential presence of crystallized minerals in polished samples can be identified quickly via reflected light microscopy. In a piece of Oued Awlitis 001 with a polished surface of ~5 x 5 mm in size a total of three shock melt pockets and one shock melt vein were observed. The needle shaped minerals crystallized from all three isolated, roundish, shock melt pockets, but are not observed in the shock melt vein, the latter apparently represents a three dimensional melt sheet.

These needle-shaped crystals provided Raman spectra with peaks at 280, 420, 500, 618, and 912 cm^{-1} (Fig. 4), and a shoulder indicating an additional peak at ~850 cm^{-1}. The Raman spectra obtained from the needles are in good agreement with Raman spectra reported for synthetic $CaAl_4Si_2O_{11}$ with characteristic peaks at 280, 422, 486, 616, 851, and 910 cm^{-1} Raman shift

(Beck et al. 2004). The broad band at 1015 cm^{-1}, together with some contribution around 460-550 cm^{-1}, is interpreted to be from the Ca-, Al-, and Si-rich glass surrounding the crystals. A 1015 cm^{-1} band was also observed and relates to the non-bridging vibrations of TO_4 tetrahedra (where T = Si, Al), and its position indicates preferentially more non-bridging Si-O than Al-O tetrahedra compared to anorthite glass with a band at 985 cm^{-1} (Sharma et al. 1983; Matson et al. 1986). The shock melt pocket of anorthite-like composition (Table 1) displays Raman spectra with a broad feature around 985 cm^{-1} (Fig. 4). In BSE images the brighter needles are surrounded by a dark halo. The halo is Al-depleted and Si-enriched compared to the anorthitic shock melt pocket, due to crystallization of the Al-rich needle-shaped crystals (Table 1). The halo contains 20 wt% Al_2O_3 suggesting an incomplete crystallization sequence. Notably, the glass is not dissociated in phases such as SiO_2, CaO or $CaSiO_3$, as revealed by the absence of Raman features in the ~800 cm^{-1} spectral region typical for SiO_2 glass.

Transmission electron microscopy investigation showed that all needles are embedded in a completely amorphous glassy matrix. No other minerals, such as garnet, corundum, kyanite, or stishovite were found in the studied shock melt pockets with TEM investigations, elemental maps, and Raman spectroscopic surveys. An average of ten TEM EDS-analyses of the CAS needles yielded a chemical composition of 52.7 wt% Al_2O_3, 32.6 wt% SiO_2, and 15.0 wt% CaO (Table 2). The empirical formula calculated on the basis of 7 cations is $Ca_{1.02}Al_{3.92}Si_{2.06}O_{11}$. The analytical results show full occupation of Ca and only very slight excess of Si and deficiency of Al with respect to the stoichiometric composition. Sodium, K, Mg, and Fe contents are below the detection limit of about 1 wt%.

The crystal structure of the new mineral was determined from eight datasets obtained with TEM using 3D ED Fig. 5; Table 3). The lattice parameters are *a* = 5.42(1) Å; *c* = 12.70(3) Å; *V* = 323(4) Å^3; Z = 2. The hexagonal structure with a space group of $P6_3/mmc$ is identical to that of the CAS phase synthesized at pressures >14 GPa and temperatures >1773 K (Table 3; Irifune et al. 1994; Gautron et al. 1999). Moreover, the atomic distribution, inferred from the combination of bond distances and bond valence sums, is also identical (Table 4). The results presented here are from the dataset 180520-2, which was refined dynamically to *R1(obs)* = 8.95% (Table 5). The crystal structure is composed of di-octahedral M1 layers containing Al and Si in 1:2 proportion, and an interlayer consisting of M2 octahedral positions fully occupied by Al, tetrahedral (T) positions half occupied by Al, and larger cavities occupied by Ca (Fig. 6). The tetrahedral position T-Al3 is disordered between two positions. An ordered model can be built with only one of the two positions occupied. The space group of such a model is $P6_3mc$, and its refinement gave slightly increased figures of merit. This result confirms that the structure is indeed centro-symmetric with a disordered tetrahedral position. The chemical composition derived from the structure model is $CaAl_4Si_2O_{11}$, in good agreement with the measured chemical composition of $Ca_{1.02}Al_{3.92}Si_{2.06}O_{11}$.

DISCUSSION

The natural CAS phase ($CaAl_4Si_2O_{11}$) presented in this study is named donwilhelmsite (IMA2018-113; Fritz et al. 2019a), and the holotype is catalogued as NHMV-O104 and preserved in the meteorite collection of the NHMV. Donwilhelmsite is named to honor Dr. Don E. Wilhelms for his seminal and ground-breaking work on the geological history of the Moon (Wilhelms 1987, 1993).

Donwilhelmsite [$CaAl_4Si_2O_{11}$] was identified within the lunar meteorite Oued Awlitis, 001, and the structure was solved by 3D electron diffraction. The needle shaped minerals are structurally and chemically identical to the CAS phase, first synthesized in static pressure experiments by Irifune et al. (1994), and later characterized in detail by Gautron et al. (1999). Similar and more Na-rich examples of the $CaAl_4Si_2O_{11}$ – $NaAl_3Si_3O_{11}$ solid solution series were previously reported form shock melt veins in basaltic Martian meteorites (Beck et al. 2004). The Na-rich endmember ($NaAl_3Si_3O_{11}$) is energetically in disfavor compared to jadeite or calcium ferrite and, thus, unlikely to form (Akaogi et al. 2010). The phases along the $CaAl_4Si_2O_{11}$ – $NaAl_3Si_3O_{11}$ solid solution series are Al-rich and Si-poor compared to the $CaAl_2Si_{3.5}O_{11}$ high-pressure phase zagamiite (Ma and Tschauner 2017; Ma et al. 2017). Donwilhelmsite forms a complex solid solution series with multiple cation substitution mechanisms including Fe, Mg, K, and Na (Irifune et al. 1994; Beck et al. 2004; Akaogi et al. 2010; El Goresy et al. 2013).

In the feldspathic lunar meteorite Oued Awlitis 001, the shock effects in plagioclase (Ferrière et al. 2017; Wittmann et al. 2019) indicate whole rock shock pressures of 20-24 GPa (Fritz et al. 2019b). The resulting shock-induced temperature increase of less than 100 K provides sufficiently low whole rock temperatures after shock decompression for the preservation of high-pressure phases when pressure almost instantly drops to zero pressure conditions (Fritz et al. 2017). In the up to 200 µm diameter sized isolated shock melt pockets, the shock pressure and temperature, preserved for a short time (milliseconds), mimic the pressure and temperature conditions in parts of the Earth's mantle. In the short period of declining temperature and pressure, donwilhelmsite grains crystallized from the melt. An Al2O3 content of ~20 wt% in the glass surrounding donwilhelmsite indicates an incomplete crystallization sequence, and the high Al-abundance suppressed the formation of the SiO_2 high-pressure polymorph stishovite.

On Earth, donwilhelmsite (the CAS phase, $CaAl_4Si_2O_{11}$) is an important mineral in continental-derived sediments subducted into the deep mantle. Static pressure experiments showed that the minimum pressure to form donwilhelmsite is 13 GPa for a $CaAl_4Si_2O_{11}$ composition (Akaogi et al. 2009) and 12 GPa for a less aluminum-rich lunar anorthositic-like composition (Nishi et al. 2018). For compositions corresponding to terrigenous sediments and upper continental crust, donwilhelmsite becomes stable at a pressure of 15.6 GPa (460 km depth) along the transition zone of the adiabatic curve (Irifune et al. 1994; Stixrude et al. 2009). Donwilhelmsite was also recorded in basaltic compositions in near- and super-solidus conditions at about 26 GPa (Hirose and Fei 2002), and up to 3% of the mineral might be present in basalts in the lowermost 100 km of the transition zone at temperatures near and above the ambient mantle adiabatic curve (Litasov and Ohtani 2005).

Whereas the mineral with a bulk composition of $CaAl_4Si_2O_{11}$ (Akaogi et al. 2009) persists to about 36 GPa (950 km depth), at ambient adiabatic conditions (Stixrude et al. 2009) its stability is limited to about 30 GPa (810 km depth) for a composition resembling lunar anorthosites (Nishi et al. 2018). The pressure regime of the Earth's mantle, however, prevents the formation of primary anorthositic magma ocean crust and the accumulation of dense residual melts and associated cumulates in the uppermost mantle (Trønnes et al. 2019). On Earth, aluminum, volatiles, and other elements incompatible in mantle minerals are recycled into the deep mantle via terrigenous and pelagic sediments that plunge down with sinking oceanic plates (Irifune et al. 1994; Plank and Langmuir 1998).

Within its stability range of about 460-700 km depth, donwilhelmsite comprises 7-10% of terrigenous sediments subducted into the deep mantle and is an important reservoir for Al, Ca, Na, K, and other large-ion lithophile trace elements (Irifune et al. 1994; Litasov and Ohtani 2005). The decompression breakdown in ascending mantle plumes of donwilhelmsite into minerals such as garnet, kyanite, and clinopyroxene might trigger minor partial melting at about 460 km deep, releasing a range of incompatible minor and trace elements. Such melts could be important agents of mantle metasomatism and contribute to the composition of ocean island basalts and kimberlites.

IMPLICATIONS

Donwilhelmsite [$CaAl_4Si_2O_{11}$], is a new high-pressure Ca-Al-silicate found in shock melt pockets in the feldspathic lunar meteorite Oued Awlitis 001. The crystal structure of donwilhelmsite was solved with precession assisted 3D ED. The 3D ED approach to solve the crystal structure of minerals, first used by Rozhdestvenskaya et al. (2010), is now often applied to characterize synthetic high-pressure phases of geological interest (Gemmi et al. 2016). Here, for the first time, 3D ED technique is used to characterize an extraterrestrial mineral. The method provides new opportunities to study the great variety of minerals with submicrometer size that formed in a broad range of exotic environments (with varying P-T-t) as represented in some meteorites, and in material brought to Earth by “sample-return” space missions.

The identification of donwilhelmsite in a lunar meteorite underlines that high-pressure phase formation in localized zones of shock melt in meteorites is a common phenomenon. Meteorites serve as ideal natural crucibles for high-pressure mineral research because 1) they can provide localized zones of shock melt with a broad range of chemical and mineralogical properties, and 2) they were protected from various types of alteration processes in the space environment.

The natural occurrence of high-pressure phases is an important asset to understand geological processes affecting the magmatic evolution of terrestrial planets, such as phase-transformations in planetary interiors, magma ocean crystallisation, and plate tectonics. In the Earth's mantle, donwilhelmsite forms during deep recycling of aluminous crustal materials, which in addition are rich in volatiles and other elements incompatible in mantle minerals. In the terrestrial rock cycle, donwilhelmsite is an important agent for storing crustal sediments between the transition zone and the uppermost lower Earth's mantle (460-700 km) over billions of years. The decompression breakdown of donwilhelmsite in pelagic and terrigenous derived components in ascending mantle plumes contributes to the EM1 and EM2 geochemical signatures recognized in various mantle derived volcanic lithologies.

ACKNOWLEDGEMENTS

The crystallographic part of this study was performed using instruments of the ASTRA laboratory established within the Operation program Prague Competitiveness (project CZ.2.16/3.1.00/24510), and the infrastructure CzechNanoLab under project LM2018110 of the Czech Ministry of Education, Youth and Sports. We acknowledge financial support for VAF through the DFG research grant FE 1523/3-1 and via a Marie Skłodowska Curie Fellow, funded by the EU-Commission, HORIZON2020 Programme, project number 749815. CEED is funded by CoE-grant 223272 from the Research Council of Norway. Skillful FIB preparation by Anja Schreiber (GFZ) is greatly acknowledged. The thin and thick sections of the Oued Awilits 001 meteorite investigated here were prepared by Goran Batic (NHMV). The meteorite fragment was acquired by the NHMV thanks to money raised in a crowdfunding campaign by L.F. and with generous support from The Barringer Crater Company. We thank Victor Sharygin, an anonymous reviewer, and the technical editor for helpful reviews that improved the quality of this contribution.

REFERENCES CITED

Akaogi, M., Haraguchi, M., Nakanishi, K., Ajiro, H., and Kojitani, H. (2010) High-pressure phase relations in the system $CaAl_4Si_2O_{11}$–$NaAl_3Si_3O_{11}$ with implication for Na-rich CAS phase in shocked Martian meteorites. Earth and Planetary Science Letters, 289, 503–508. doi.org/10.1016/j.epsl.2009.11.043

Akaogi, M., Haraguchi, M., Yaguchi, M., and Kojitani, H. (2009) High-pressure phase relations and thermodynamic properties of $CaAl_4Si_2O_{11}$ CAS phase. Physics of the Earth and Planetary Interiors, 173, 1–6. doi.org/10.1016/j.pepi.2008.10.010

Beck, P., Gillet, P., Gautron, L., Daniel, I., and El Goresy, A. (2004) A new natural high-pressure (Na,Ca)-hexaluminosilicate $[(Ca_xNa_{1-x})Al_{3+x}Si_{3-x}O_{11}]$ in shocked Martian meteorites. Earth and Planetary Science Letters, 219, 1–12. doi.org/10.1016/S0012-821X(03)00695-2

Chen M., Sharp T.G., El Goresy A., Wopenka B., and Xie X. (1996) The majorite pyrope magnesiowustite assemblage: Constraints on the history of shock veins in chondrites. Science, 271, 1570–1573. doi.org/10.1126/science.271.5255.1570

Delavault, H., Chauvel, C., Thomassot, E., Devey, C. W., and Dazas, B. (2016) Sulfur and lead isotopic evidence of relic Archean sediments in the Pitcairn mantle plume. Proceedings of the National Academy of Sciences of the United States of America, 113, 12952–12956. doi.org/10.1073

El Goresy A., Gillet P., Miyahara M., Ohtani E., Ozawa S., Beck P., and Montagnac G. (2013) Shock-induced deformation of Shergottites: Shock–pressures and perturbations of magmatic ages on Mars. Geochimica et Cosmochimica Acta, 101, 233–262. doi.org/10.1016/j.gca.2012.10.002

Fernandes, V.A., Fritz, J., Weiss, B., Garrick-Bethell, I., and Shuster, D. (2013) The bombardment history of the Moon as recorded by ^{40}Ar-^{39}Ar chronometry. Meteoritics & Planetary Science, 48, 241–269. doi.org/10.1111/maps.12054

Ferrière, L., Meier, M.M.M., Assis Fernandes, V., Fritz, J., Greshake, A., Barrat, J.-A., Böttger, U., Bouvier, A., Brandstätter, F., Busemann, H., Korotev, R.L., Maden, C., Magna, T., Schmitt-Kopplin, Ph., Schrader, D.L., and Wadhwa, M. (2017) The unique crowdfunded Oued Awlitis 001 lunar meteorite – A consortium overview. 48th Lunar Planetary Science Conference, abstract #1621.

Fritz, J., Greshake, A., and Fernandes, V. (2017) Revising the shock classification of meteorites. Meteoritics & Planetary Science, 52, 1216–1232. doi.org/10.1111/maps.12845

Fritz, J., Greshake, A., Klementova, M., Wirth, R., Palatinus, L., Assis Fernandes, V., Böttger, U., and Ferrière, L. (2019a) Donwilhelmsite, IMA 2018-113. CNMNC Newsletter No. 47, February 2019, page 199. European Journal of Mineralogy, 31, 197–202.

Fritz, J., Fernandes, V., Greshake, A., Holzwarth, A., and Böttger, U. (2019b) On the formation of diaplectic glass: Shock and thermal experiments with plagioclase of different chemical compositions. Meteoritics & Planetary Science, 54, 1533–1547. doi.org/10.1111/maps.13289

Garapić G., Jackson, M.G., Hauri, E.H., Hart, S.R., Farley, K.A., Blusztajn, J.S., and Woodhead, J.D. (2015) A radiogenic isotopic (He-Sr-Nd-Pb-Os) study of lavas from the Pitcairn hotspot: Implications for the origin of EM-1 (enriched mantle 1). Lithos, 228–229, 1–11. doi.org/10.1016/j.lithos.2015.04.010

Gautron, L., Angel, R.J., and Miletich, R. (1999) Structural characterisation of the high-pressure phase $CaAl_4Si_2O_{11}$. Physics and Chemistry of Minerals, 27, 47–51. doi.org/10.1007/s002690050239

Gemmi, M. Merlini, M., Palatinus, L., Fumagalli, P., and Hanfland, M. (2016) Electron diffraction determination of 11.5 Å and HySo structures: Candidate water carriers to the Upper Mantle. American Mineralogist, 101, 2645.

Gemmi, M. Mugnaioli, E., Gorelik, T.E., Kolb, U., Palatinus, L., Boullay, P., Hovmöller S, and Abrahams, J.P. (2019) 3D Electron Diffraction: The nanocrystallography tevolution. ACS Central Science, 5, 1315−1329. doi.org/ 10.1021/acscentsci.9b00394

Hirose, K., and Fei, Y. (2002) Subsolidus and melting phase relations of basaltic composition in the uppermost lower mantle. Geochimica et Cosmochimica Acta, 66, 2099–2108. doi.org/10.1016/S0016-7037(02)00847-5

Irifune, T., Ringwood, A.E., and Hibberson, W.O. (1994) Subduction of continental crust and terrigenous and pelagic sediments: an experimental study. Earth and Planetary Science Letters, 126, 351–368. doi.org/10.1016/0012-821X(94)90117-1

Jarosewich E., Nelen J.A., and Norberg J.A. (1980) Reference samples for electron microprobe analysis. Geostandard Newsletters, 4, 43–47.

Kolb, U., Gorelik, T., and Otten, M.T. (2008) Towards automated diffraction tomography: Part II - Cell parameter determination. Ultramicroscopy, 108, 763–772. doi.org/10.1016/j.ultramic.2007.12.002

Litasov, K.D., and Ohtani, E. (2005) Phase relations in hydrous MORB at 18–28 GPa: implications for heterogeneity of the lower mantle. Physics of the Earth and Planetary Interiors, 150, 239–236. doi.org/10.1016/j.pepi.2004.10.010

Ma, C., and Tschauner, O. (2017) Zagamiite. IMA 2015-022a. CNMNC Newsletter No. 36, April 2017, Mineralogical Magazine, 81, 409.

Ma, C., Tschauner, O., and Beckett, J.R. (2017) A new high-pressure calcium aluminosilicate ($CaAl_2Si_{3.5}O_{11}$) in martian meteorites: another after-life for plagioclase and connections to the CAS phase. 48th Lunar Planetary Science Conference, abstract #1128.

Matson, D.W., Sharma, S.K., and Philpotts, J.A. (1986) Raman spectra of some tectosilicates and of glasses along the orthoclase-anorthite and nepheline-anorthite joins. American Mineralogist, 71, 694–704.

Mugnaioli, E., Gorelik, T., and Kolb, U. (2009) "Ab initio" structure solution from electron diffraction data obtained by a combination of automated diffraction tomography and precession technique. Ultramicroscopy, 109, 758–765. doi.org/10.1016/j.ultramic.2009.01.011

Nishi, M., Gréaux, S., Tateno, S., Kuwayama, Y., Kawai, K., Irifune, T., and Maruyama, S. (2018) High-pressure phase transitions of anorthosite crust in the Earth's deep mantle. Geoscience Frontiers, 9, 1859–1870. doi.org/10.1016/j.gsf.2017.10.002

Palatinus, L., Bráyda, P., Jelínek, M., Hrdá, J., Steciuk, G., and Klementová, M. (2019) Specifics of the data processing of precession electron diffraction tomography data and their implementation in the program PETS2.0. Acta Crystallographica, B75, 512–522. doi.org/10.1107/S2052520619007534Palatinus, L., and Chapuis, G. (2007) SUPERFLIP - a computer program for the solution of crystal structures by charge flipping in arbitrary dimensions. Journal of Applied Crystallography, 40, 786–790. doi.org/10.1107/S0021889807029238

Palatinus, L., Petříček, V., and Corrêa, C.A. (2015a) Structure refinement using precession electron diffraction tomography and dynamical diffraction: theory and implementation. Acta Crystallographica, A71, 235–244. doi.org/10.1107/S2053273315001266

Palatinus, L., Corrêa, C.A., Steciuk, G., Jacob, D., Roussel, P., Boullay, P., Klementová, M., Gemmi, M., Kopeček, J., Domeneghetti, M.C., Cámara, F., and Petříček, V. (2015b) Structure refinement using precession electron diffraction tomography and dynamical diffraction: tests on experimental data. Acta Crystallographica, B71, 740–751. doi.org/10.1107/S2052520615017023

Pearson D.G., Brenker, F.E., Nestola, F., McNeill, J., Nasdala, L., Hutchison, M.T., Matveev S., Mather, K., Silversmit, G., Vekemans, B., Schmitz, S., Vekemans, B., and Vincze, L. (2014) Hydrous mantle transition zone indicated by ringwoodite included within diamond. Nature, 507, 221–224. doi.org/10.1038/nature13080

Petříček, V., Dušek, M., and Palatinus, L. (2014) Crystallographic computing system JANA2006: general features. Zeitschrift für Kristallographie - Crystalline Materials, 229-5, 345–352. doi.org/10.1515/zkri-2014-1737

Plank T., and Langmuir, C.H. (1998) The chemical composition of subducting sediment and its consequences for the crust and mantle. Chemical Geology, 145, 325–394. doi.org/10.1016/S0009-2541(97)00150-2

Poli, S., and Schmidt, M.W. (2002) Petrology of subducted slabs. Annual Review of Earth and Planetary Sciences, 30, 207–235. doi.org/10.1146/annurev.earth.30.091201.140550

Rozhdestvenskaya, I., Mugnaioli, E., Czank, M., Depmeier, W., Kolb, U., Reinholdt, A., and Weirich, T. (2010) The structure of charoite, $(K,Sr,Ba,Mn)_{15-16}(Ca,Na)_{32}[(Si_{70}(O,OH)_{180})](OH,F)_{4.0}.nH_2O$, solved by conventional and automated electron diffraction. Mineralogical Magazine, 74, 159–177. doi.org/10.1180/minmag.2010.074.1.159

Ruzicka, A., Grossman, J., Bouvier, A., and Agee, C.B. (2017) The Meteoritical Bulletin, No. 103, Meteoritics & Planetary Science, 52, 1014.

Sharma, S.K., Simons, B., and Yoder, H.S. (1983) Raman study of anorthite, calcium Tschermak's pyroxene, and gehlenite in crystalline and glassy states. American Mineralogist, 68, 1113–1125.

Smith, J.V. Anderson, A.T., Newton, R.C., Olsen, E.J., Wyllie, P.J., Crewe, A.V., Isaacson, M. S., and Johnson, D. (1970) Petrologic history of the Moon inferred from petrography, mineralogy and petrogenesis of Apollo 11 rocks. Proceedings of the Apollo Eleven Lunar Science Conference, 897–925. https://resolver.caltech.edu/CaltechAUTHORS:20160209-101343274

Stixrude, L., Koker, N. de, Sun, N., Mookherjee, M., and Karki, B.B. (2009) Thermodynamics of silicate liquids in the deep Earth. Earth and Planetary Science Letters, 278, 226–232. doi.org/10.1016/j.epsl.2008.12.006

Tomioka, T., and Miyahara, M. (2017) High-pressure minerals in shocked meteorites. Meteoritics & Planetary Science, 52, 2017–2039. doi.org/10.1111/maps.12902

Trønnes, R.G., Baron, M.A., Eigenmann, K.R., Guren, M. G., Heyn, B.H., Løken, A. and Mohn, C.E. (2019) Core formation, mantle differentiation and core-mantle interaction within

Earth and the terrestrial planets. Tectonophysics, 760, 165–198. doi.org/10.1016/j.tecto.2018.10.021

White, W.M. (2015) Isotopes, DUPAL, LLSVPs, and Anekantavada. Chemical Geology, 419, 10–28. doi.org/10.1016/j.chemgeo.2015.09.026

Wieczorek, M.A., Jolliff, B.L., Khan, A., Pritchard, M.E., Weiss, B.P., Williams, J.G., Hood, L.L., Righter, K., Neal, C.R., Shearer, C.K., McCallum, I.S., Tompkins, S., Ray Hawke, B., Peterson, C., Gillis, J.J., and Bussey, B. (2006) The constitution and structure of the lunar interior. Reviews in Mineralogy and Geochemistry, 60 (1), 221–364. doi.org/10.2138/rmg.2006.60.3

Wilhelms, D.E. (1987) The geological history of the Moon. US Geological Survey Professional Paper 1348, pp 302. doi: 10.3133/pp1348

Wilhelms, D.E. (1993) To a rocky Moon: A geologist's history of lunar exploration. The University of Arizona Press, pp. 477.

Wittmann, A., Korotev, R.L., Jolliff, B.L., Nishiizumi, K., Jull, A.J.T., Caffee, M.W., Zanetti M., and Irving, A.J. (2019) Petrogenesis of lunar impact melt rock meteorite Oued Awlitis 001. Meteoritics & Planetary Science, 54, 2167–2188. doi.org/10.1111/maps.13218

Wood, J., Dickey, J.S.Jr., Marvin, U., and Powell, B.N. (1970) Lunar anorthosites. Science, 167, 602–604. doi.org/10.1126/science.167.3918.602

Figure captions

Figure 1: Backscattered-electron (BSE) image showing a petrographic overview of the lunar meteorite Oued Awlitis 001 (NHMV-O104). Large plagioclase clasts (pl clast) are embedded in a matrix composed of olivine (ol), pyroxene (px), plagioclase (pl), and silica (not indicated).

Figure 2: Backscattered-electron (BSE) image showing a) a shock melt pocket with needles of donwilhelmsite. The grey host rock is mainly composed of anorthite with bright minerals representing olivine and pyroxene. Dark regions are cracks on the surface of the polished thick section. b) BSE image showing bundles of needle-like (acicular) donwilhelmsite crystallized in a ~100 µm wide shock melt pocket of anorthitic chemical composition. The donwilhelmsite needles are surrounded by a darker halo. c) Bright field TEM image showing an almost defect free donwilhelmsite crystal. The dark upper left corner is the platinum strip holding the sample.

Figure 3: Ca, Al, and Fe elemental maps and backscattered electron (BSE) image showing needles of donwilhelmsite within a shock melt pocket. Elemental maps of Fe and Mg (not shown) reveal chemical inhomogeneity within the anorthositic-like shock melt pocket, likely related to melted pyroxene or olivine grains.

Figure 4: Raman spectra of donwilhelmsite and the glass composing the shock melt pocket. The donwilhelmsite spectra shows peaks at 280, 420, 500, 618, 850, and 912 cm^{-1} together with spectral contributions from the surrounding glass halo providing broad features in the 500 to 560 region and at ~1015 cm^{-1} Raman shift. The shock melt pocket displays a Raman spectra with broad hump with maxima at ~500 and ~560 cm^{-1} and a broad hump with a maxima at ~985 cm^{-1} Raman shift.

DOI: https://doi.org/10.2138/am-2020-7393

Figure 5: Precession electron diffraction tomography (PEDT). Displayed are sections through the experimental diffraction dataset 180520-2 in three orientations with the unit cell marked.

Figure 6: Structure of donwilhelmsite. a) The structure is composed of b) octahedral M1-layers (dark blue) occupied by Al and Si in 1:2 ratio. c) The interlayers, contain octahedral M2-positions (grey) fully occupied by Al, tetrahedral positions (T, grey) half occupied by Al, and cavities occupied by Ca (green).

Table 1 | Chemical composition of the shock melt pocket given as an average of 10 electron microprobe analyses (Melt) and their standard deviation (S.D.). The chemical composition of the glass halo rimming donwilhelmsite (Gl) and for donwilhelmsite (DW) were obtained by TEM-EDS analytics.

	Melt	S.D.	Gl	DW
SiO_2	44.0	0,75	60.7	32.6
Na_2O	0.35	0.06		
TiO_2	0.10	0.04		
K_2O	0.01	0.01		
Cr_2O_3	0.04	0.02		
Al_2O_3	35.4	1.23	20.8	52.7
MgO	0.52	0.18		
MnO	0.01	0.02		
CaO	18.9	0.51	18.5	15.0
FeO	1.09	0.34		
Total	100.4	0.41	100.0	100.3

Table 2 │ Chemical data (in *weight % of oxides* and *atoms per formula unit* = *apfu*). For donwilhelmsite, the empirical formula as calculated on the basis of 7 cations is $Ca_{1.02}Al_{3.92}Si_{2.06}O_{11}$, and the simplified formula is $CaAl_4 Si_2 O_{11}$.

	Al_2O_3 wt%	**SiO_2** wt%	**CaO** wt%	**Al** 7 apfu	**Si** 7apfu	**Ca** 7 apfu
sp-01	52.3	32.1	15.7	3.9	2.0	1.1
sp-02	54.0	32.6	14.1	4.0	2.1	1.0
sp-03	46.8	35.2	17.7	3.5	2.3	1.2
sp-04	52.9	34.1	13.9	3.9	2.1	0.9
sp-05	54.0	32.2	14.3	4.0	2.0	1.0
sp-06	51.5	33.1	15.6	3.8	2.1	1.1
sp-07	52.8	32.7	14.9	3.9	2.1	1.0
sp-08	53.3	31.0	15.6	40	2.0	1.1
sp-09	53.2	31.6	15.3	4.0	2.0	1.0
sp-10	56.0	31.4	13.3	4.1	2.0	0.9
average	52.7	32.6	15.0	3.9	2.1	1.0
std. dev.	2.4	1.3	1.2	0.2	0.1	0.1
min.	46.8	31.0	13.3	3.5	2.0	0.9
max.	56.0	35.2	17.7	4.1	2.3	1.2

Table 3 │ Comparison of crystal data with hexagonal crystal system. Diffraction data of the here described new mineral was determined by precession electron diffraction tomography (PEDT), X-ray diffraction data from Gautorn et al. (1999) are obtained on single crystals and Akaogi et al. (2009) used powder samples. The synchrotron diffraction patterns of micrometer-sized high aluminum silica (HAS) zagamiite grains were consider similar to powder-like samples (Ma et al. 2017). The cell parameters of these hexagonal crystals are given as *a* and *c* in [Å] Angstrom and the cell volume V = a^2c sin(60°) in [$Å^3$]. The numbers in parentheses () represent the estimated standard deviations in the last digit. *Unit cell parameters from electron diffraction tomography (EDT) are known to have distortions and lower accuracy (Kolb et al., 2008). Z is the number of formula units per unit cell. The calculated density of donwilhelmsite is 3.903 [g/cm^{-3}].

Composition	Space group	*a* [Å]	*c* [Å]	*V* [$Å^3$]	*Z*	Reference
Donwilhelmsite $CaAl_4Si_2O_{11}$	*P*6_3/*mmc*	5.42 (1)	12.70 (3)*	323(4)	2	This work
synthetic $CaAl_4Si_2O_{11}$	*P*6_3/*mmc*	5.4223 (4)	12.7041 (6)	323.28 (5)	2	Gautron et al. 1999
synthetic $CaAl_4Si_2O_{11}$	*P*6_3/*mmc*	5.4239 (2)	12.6805 (5)	323.06 (3)	2	Akaogiet al. 2009
Zagamiite $CaAl_2Si_{3.5}O_{11}$	*P*6_3/*mmc*	5.403 (2)	12.77 (3)			Ma et al. 2017

Table. 4 │ Characteristics of cation coordination.

position	occupancy	BVS[1]	ECON[2]	average distance to coordinating oxygen atoms [Å]	*average distance of synthetic CAS [Å] [2]*
Ca	Ca	1.816(3)	11.8945	2.6723	*2.671*
M1	Si1 (2/3)	3.513(7)	5.9876	1.8325	*1.833*
	Al1 (1/3)	3.61(1)			
M2	Al2	2.956(6)	5.6976	1.9159	*1.918*
T	Al3 (1/2)	3.15(2)	3.8164	1.7456	*1.724*

[1]BVS - Bond Valence Sum; [2] ECON - Effective Coordination Number.

574 **Table. 5 │ Analytical conditions for donwilhelmsite.**

Data collection	
Radiation type	electrons, 120 kV
Wavelength [Å]	0.0335
Precession angle φ [°]	1.0
Illuminated area diameter [nm]	1 000
Resolution [Å]	0.7150
No of recorded frames	101
Completeness	100
No. of refined reflections - all/observed [I > 3σ(I)]	3 639/2 574
Dynamical structure refinement	
g^{max} [$Å^{-1}$], S_g^{max} (matrix), S_g^{max} (refine), R_{Sg}, N_{or}	1.6, 0.01, 0.1, 0.4, 128
R1(F), wR(F), GOF - (obs/all) [%]	8.95/11.91, 10.00/10.12, 4.77/4.06
No. of refined parameters	127

575 [a] $R1 = \Sigma||F_o|-|F_c||/\Sigma|F_o|$; [b] $wR = [\Sigma w(F_o^2-F_c^2)^2/\Sigma w(F_o^2)^2]^{1/2}$; [c] $GOF = [\Sigma w(F_o^2-F_c^2)^2/\Sigma$
576 $w(F_o^2)^2]^{1/2}$

577

578

579

Fig. 1

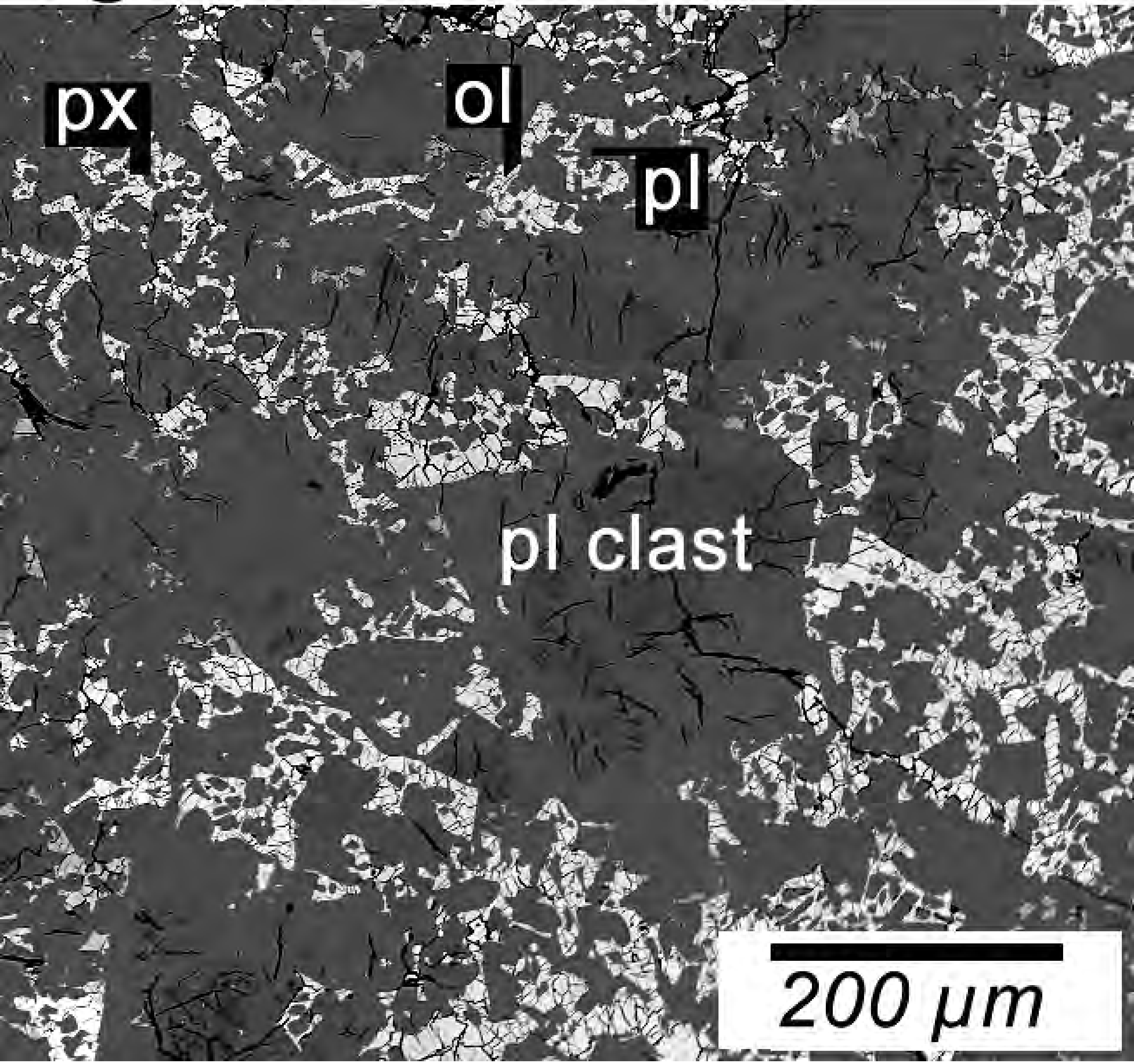

Fig. 2

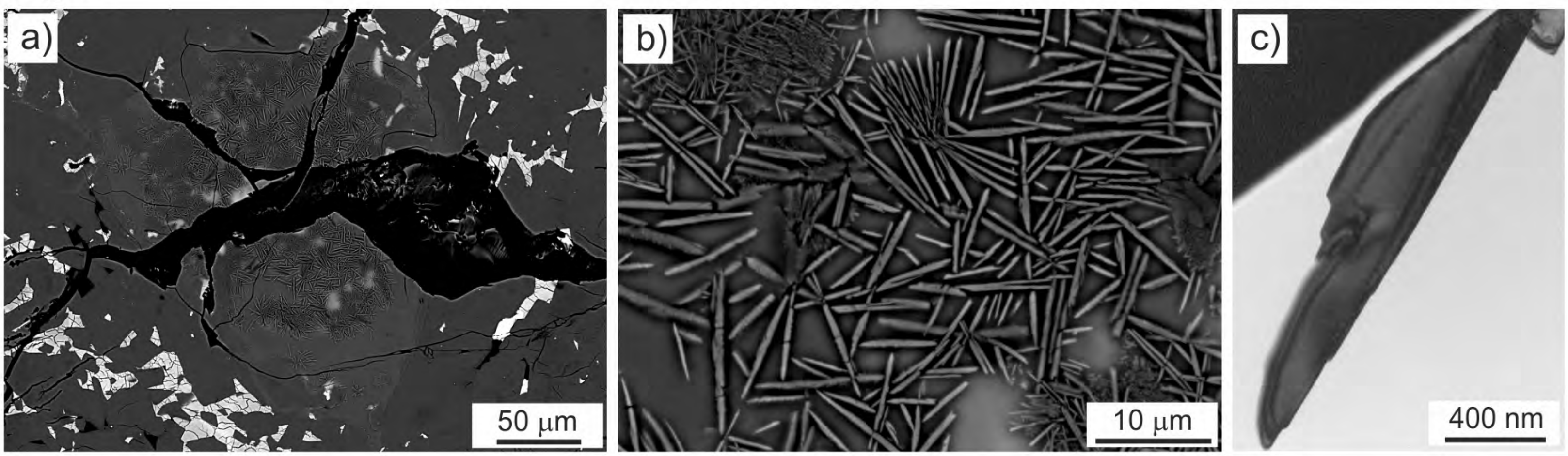

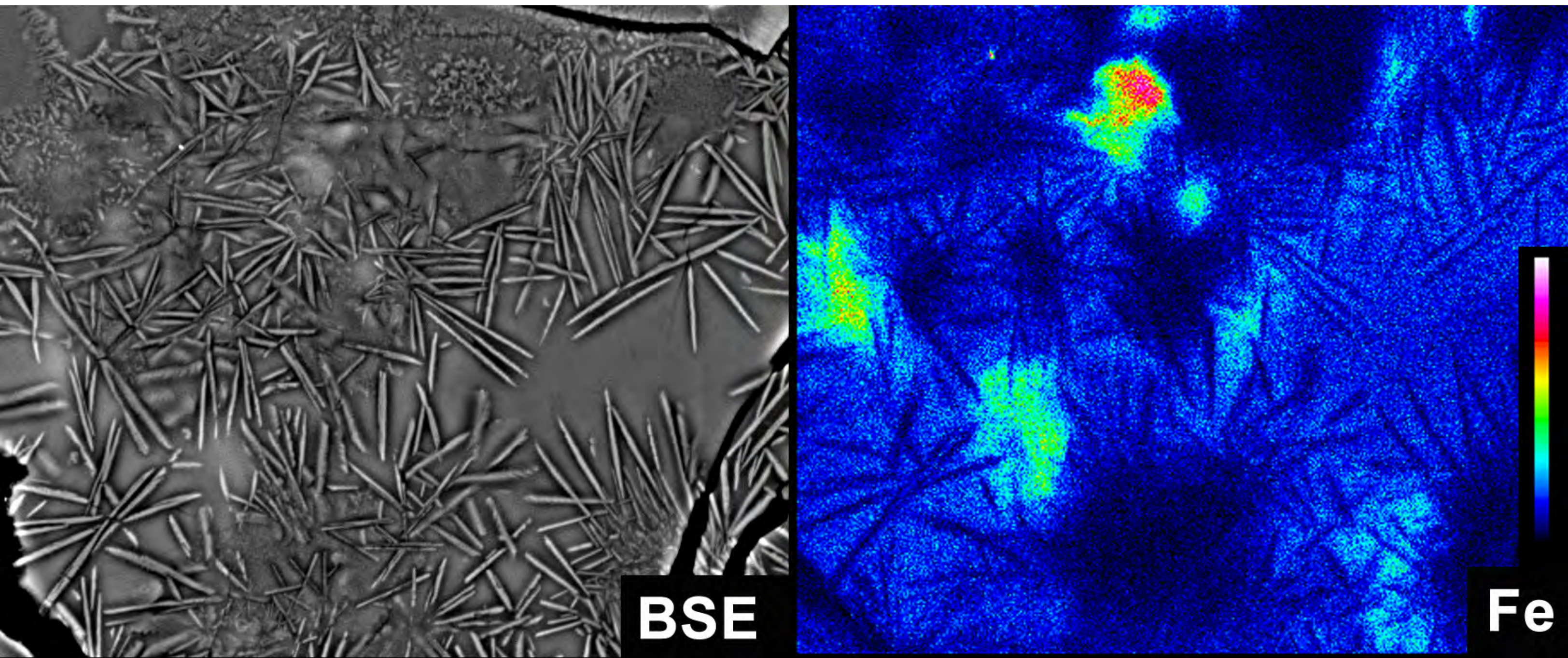

BSE
Fe
10 µm
Ca
Al

Fig. 4

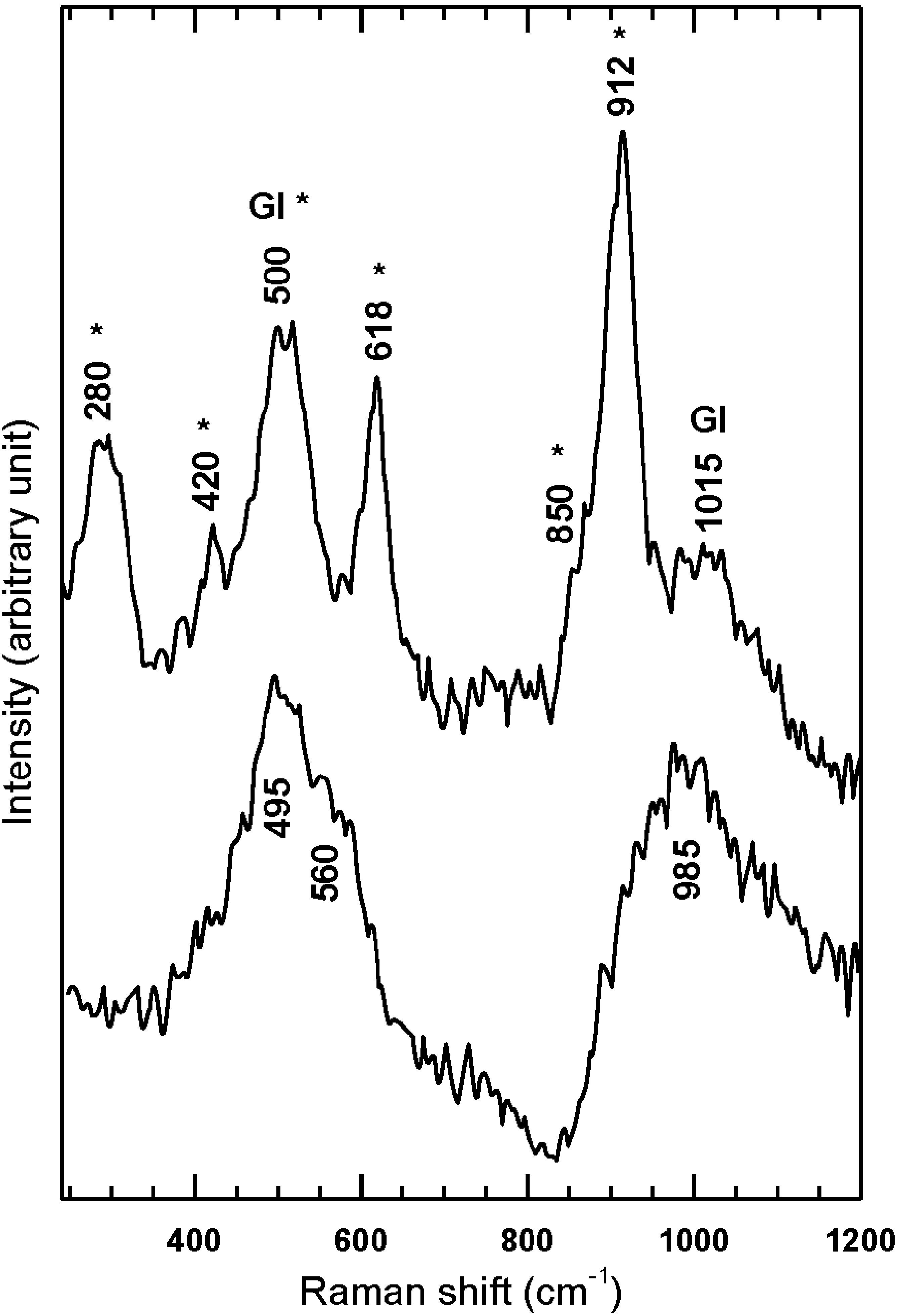

Intensity (arbitrary unit)
Raman shift (cm^{-1})
400
600
800
1000
1200
280 *
420 *
500
Gl *
618 *
850 *
912 *
1015 Gl
495
560
985

Fig. 5

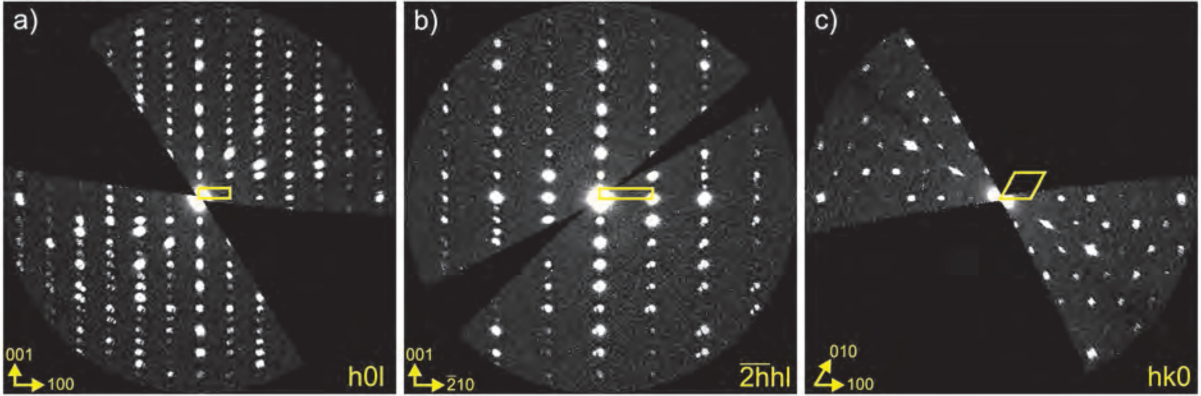

Fig. 6